Journal of Crystal Growth 404 (2014) 146–151

Contents lists available at ScienceDirect

Journal of Crystal Growth

journal homepage: www.elsevier.com/locate/jcrysgro

Molecular beam epitaxy of ferromagnetic epitaxial GdN thin films

F. Natali [a,*], S. Vézian [b], S. Granville [c], B. Damilano [b], H.J. Trodahl [a], E.-M. Anton [a], H. Warring [a], F. Semond [b], Y. Cordier [b], S.V. Chong [c], B.J. Ruck [a]

[a] MacDiarmid Institute for Advanced Materials and Nanotechnology, School of Chemical and Physical Sciences, Victoria University of Wellington, PO Box 600, Wellington, New Zealand
[b] Centre de Recherche sur l'Hétéro-Épitaxie et ses Applications (CRHEA), Centre National de la Recherche Scientifique, Rue Bernard Gregory, 06560 Valbonne, France
[c] MacDiarmid Institute for Advanced Materials and Nanotechnology, Robinson Research Institute, Victoria University of Wellington, PO Box 33436, Lower Hutt 5046, New Zealand

ARTICLE INFO

Article history:
Received 7 May 2014
Received in revised form
27 June 2014
Accepted 6 July 2014
Communicated by K.H. Ploog
Available online 15 July 2014

Keywords:
A3. Molecular beam epitaxy
B1. Nitrides
B2. Magnetic materials
B2. Semiconducting materials

ABSTRACT

The structural, magnetic and electrical properties of a series of GdN thin films grown by molecular beam epitaxy on AlN on silicon substrates have been studied. *In situ* scanning tunneling microscopy and reflection high energy electron diffraction evidence the formation of three-dimensional GdN triangle-shaped islands in the early stage of the growth which coalesce as growth develops. It is then shown by X-ray diffraction that the thickness and the growth temperature play a key role in determining the structural properties of the GdN films and optimum growth conditions are found. A significant structural dependence of the magnetic properties is observed with results suggesting superparamagnetism in very thin films while thicker films show uniform ferromagnetism.

1. Introduction

Gadolinium nitride and related rare-earth nitrides (RENs) have attracted special interest in the last few years, chiefly because of the promise they hold for applications in the field of semiconductor spintronics but also because of the opportunities they provide for fundamental studies of strongly correlated systems [1,2]. The prospect of having materials that combine the properties of both ferromagnets and semiconductors, so-called intrinsic ferromagnetic semiconductors, has fostered a substantial interest and, as a result, several groups have already succeeded in obtaining proof of concept GdN-based device structures. These include GdN-based spin-filter Josephson junctions [3,4], field effect transistor structures [5] and, most recently, the use of GdN quantum dots to enhance the efficiency of GaN tunnel junctions [6] and the development of topological insulator/GdN heterostructure devices [7]. Further interest is spurred by the fact that the RENs have structural properties compatible with the well-established group-III-nitride family, offering an opportunity to combine both technologies. The lattice mismatch between GdN and either AlN or GaN of $\sim+13\%$ and $\sim+10\%$, respectively, though relatively severe, is comparable to that in heteroepitaxial systems [8]. Even here preliminary results have been demonstrated [9–12].

At present, it is noticeable that most of the studies have been performed on the polycrystalline form of the RENs as they have been proven challenging to grow as epitaxial thin films due to difficulties such as the lack of lattice-matched substrates, their propensity to form nitrogen vacancies (V_N) and to decompose in air into rare-earth oxides. However a few recent results demonstrate that epitaxial thin films grown by molecular beam epitaxy (MBE) of not only GdN [9–12], the most widely studied REN, but also SmN [13,14] and EuN, [13,15,16], can be achieved. While the material quality is good enough to allow advances in their study towards both fundamental understanding and exploitation, the MBE growth of such compounds has not received detailed attention and many fundamental questions remain. For example, there are no clear results or consensus even on the optimum growth temperature of GdN and the surface morphology and structural properties of the material have been barely investigated.

In this letter, we report on the molecular beam epitaxy of GdN films, in particular on the influence of the thickness and the growth temperature on their structural, magnetic and electrical properties.

2. Experimental

The GdN films were grown in a Riber MBE system equipped with conventional Al, Ga and Gd, solid sources. NH_3 and molecular

* Corresponding author.
E-mail address: franck.natali@vuw.ac.nz (F. Natali).

http://dx.doi.org/10.1016/j.jcrysgro.2014.07.010
0022-0248/

nitrogen (N_2) were used as the nitrogen precursor for the growth of AlN/GaN and GdN, respectively. The observation by *in situ* reflection high-energy electron diffraction (RHEED) of the well-known $(7\times7\leftrightarrow1\times1)$ Si(111) surface phase transition was used to calibrate the temperature by adjusting the emissivity of the optical infrared pyrometer to get a transition temperature of 830 °C. The Si–rare earth (RE) reaction is very rapid and it prevents the epitaxial growth of RENs directly onto Si [9], so the GdN films were deposited onto wurtzite (0001)-oriented AlN buffer layers which were themselves grown by MBE on (111) silicon substrates [17]. The GdN layers were grown at substrate temperatures ranging from 470 to 850 °C, at a beam equivalent pressure (BEP) of 2.7×10^{-5} Torr and 5×10^{-8} Torr for N_2 and Gd, respectively, leading to a growth rate of about 0.12 ± 0.01 μm/h. It is worth mentioning that the growth of GdN, like some of the other RENs, can be carried out under pure N_2 thanks to the catalytic break-down of molecular nitrogen by RE atoms on the growing surface [9]. The GdN layers were capped with a 100–150 nm thick GaN layer to prevent decomposition in air. The crystalline structure has been assessed also by XRD $2\theta-\theta$ scans. The temperature- and field-dependence of the magnetization were measured with a superconducting quantum interference device for an in-plane field orientation. Electron transport measurements have been carried out using a van der Pauw configuration.

3. Results and discussion

In situ RHEED observations during the growth confirm the epitaxial character of the GdN films. As shown in Fig. 1(a) the RHEED pattern of a 25 nm thick GdN film deposited onto 100 nm thick (0001)AlN buffer layer measured along the [1–210] azimuth of AlN(0001) is characterized by the presence of double spots (indicated by the arrows). Note that double spots are not observable along the [1–100] azimuth in Fig. 1(b) as predicted by symmetry considerations. This observation, already reported by us and others, is characteristic of twinned domains in the fcc structure of GdN [8,9]. Fig. 1(c) and (d) displays the geometrical arrangement of diffraction spots in RHEED patterns for a (111) surface along the ⟨1–10⟩ directions of a cubic single-crystal (solid circles) and with the superimposition of a second cubic crystal rotated by 180° (open circles), respectively. This behavior is actually more general and has been described for various systems like MgO on 6H-SiC [18], ZnO on MgO [19] and MgO on GaN [20].

Thus far the RHEED technique has been relied upon to characterize the two rotational variants for the (111) GdN grains. Here, we provide new insight with a scanning tunneling microscope (STM) study giving us a real-space picture of the GdN grains and surface morphologies. Fig. 2 shows 100×100 nm^2 topographic STM images of (a) 25 nm and (b) 50 nm thick GdN films deposited at 650 °C on a 50 nm thick AlN buffer layer. Our STM study suggests average grain sizes of about 9.5 nm and 15.5 nm and root mean square (RMS) roughnesses, calculated from 200×200 nm^2 images, of about 1.1 nm and 2.2 nm for the 25 nm and 50 nm thick GdN films, respectively. We have observed that the average grain size and RMS do not change significantly for film thicknesses ranging from 10 to 25 nm. Furthermore the STM images evidence clearly the growth of "triangular shape–like islands" with their orientations rotated by 60° with respect to each other. We can see an increase of the crystallite size with increasing thickness of the GdN films, which is well correlated with the decrease of the X-ray diffraction (XRD) full width at half-maximum (FWHM) of both the GdN (111) reflection from $2\theta/\omega$ scans and the out of plane (111) rocking curve (not shown). The rocking curve FWHM is about $13''\times10^3$, $5.9''\times10^3$ and $3.6''\times10^3$ for thicknesses of ~16, 55 and 120 nm, respectively. Increasing the thickness of the GdN films improves the crystal quality, which we attribute to dislocation reaction and elimination after the coalescence of the grains or islands. Fig. 3 displays the XRD 2θ-scan of a 120 nm thick GdN film grown on a 100 nm thick AlN buffer layer. In addition to the peaks of AlN, GaN and Si we observe only the (111) and (222) reflections of GdN. Clearly the hexagonal face of AlN template favors a fully (111)-oriented GdN film. Furthermore the RHEED studies show that all epitaxial GdN layers display sixfold symmetry, implying two epitaxial orientations with the two crystal variants related by a 60° rotation.

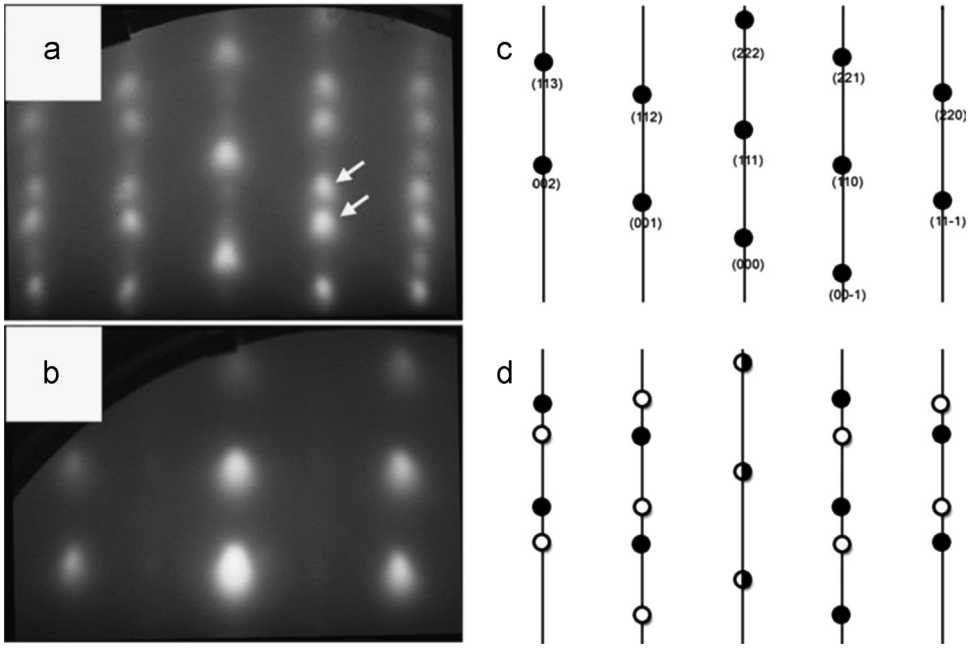

Fig. 1. RHEED patterns recorded after the growth of about 25 nm of GdN on AlN(0001), along (a) the [1–210] and (b) the [1–100] azimuths of AlN(0001). The double spots indicated by the arrows correspond to the twinned domains in the fcc structure of GdN. Geometrical arrangement of diffraction spots in RHEED patterns for a (111) surface along the ⟨1–10⟩ directions of (c) a cubic single-crystal (solid circles) and (d) with the superimposition of a second cubic crystal rotated by 180° (open circles).

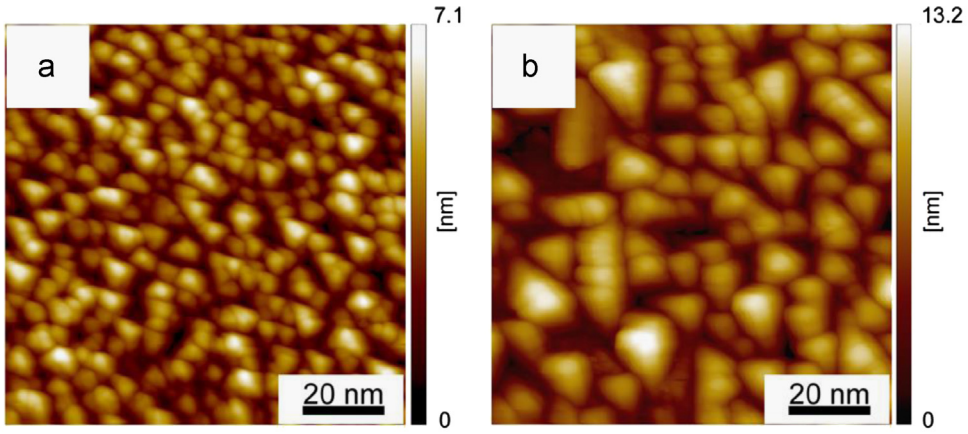

Fig. 2. $100 \times 100\ nm^2$ STM images of (a) 25 nm and (b) 50 nm thick GdN grown at 650 °C. Acquisition parameters are 0.1 nA and +2 V (sample bias).

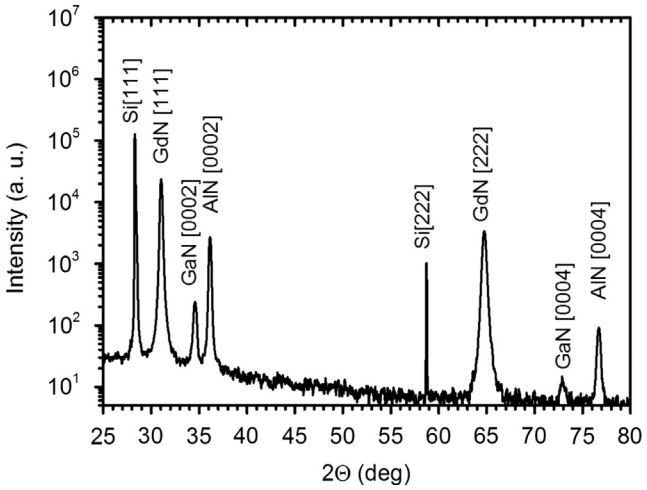

Fig. 3. Typical XRD 2θ scan of a 120 nm thick GdN layer grown on a 100 nm thick AlN template and capped with a GaN layer.

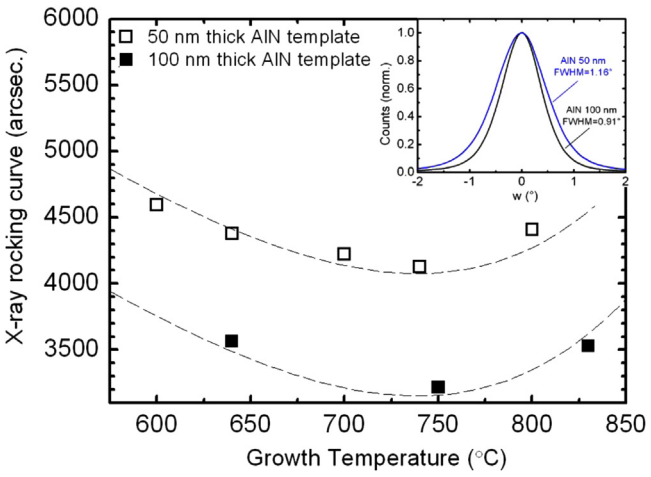

Fig. 4. Full width at half-maximum height (FWHM) of the out of plane (111) rocking curve *versus* the growth temperature of 120 nm thick GdN layer using (a) 50 nm (open squares) and 100 nm (solid squares) thick AlN(0001) template layers. The dashed lines are only a guide for the eye. The inset shows the rocking curves of a GdN layer grown on a 50 nm (blue line) and 100 nm (black line) thick AlN(0001) template layers. (For interpretation of the references to color in this figure legend, the reader is referred to the web version of this article.)

We now turn to the influence of growth temperature on the structural properties assessed by XRD of 120 nm-thick GdN films grown on 50 nm thick AlN buffer layers. The FWHM of the out of plane (111) rocking curve is reported in Fig. 4 (open squares – the dashed line is a guide for the eye). The structural properties improve when the growth temperature increases. More interesting is the influence of the AlN template quality on the subsequent growth of GdN. As observed in a lot of hetero-epitaxial systems, it is well known that for AlN films grown on silicon, the thicker the AlN film the lower the FWHM of the XRD rocking curve [21]. A significant decrease of the rocking curve width for the GdN films grown on 100 nm thick AlN templates (solid squares) is observed. In addition, the FWHM *versus* growth temperature follows the same qualitative trend as the one measured for GdN films grown on 50 nm thick AlN template. This indicates that there is a major limitation for reducing the thickness of the AlN buffer layer. The inset of Fig. 4 shows the XRD rocking curve for the samples grown at 750 °C on a 50 nm thick AlN template (blue line) and on a 100 nm thick AlN template (black line). Interestingly, we can see that whatever the AlN thickness, the GdN quality tends to become poorer for growth temperatures above 750 °C. At this stage the reason for this marginal deterioration is unknown, but it is worth noting that at this temperature we expect neither Gd adatoms nor GdN to re-evaporate. However, a substantial concentration of nitrogen vacancies is likely to form at high growth temperature conditions due to their small formation energy on the order of 0.5 eV [22]. Such defects have already been demonstrated to influence the ferromagnetism and electrical properties of RENs [23–25] and we may speculate that they, at some concentration level, lead also to the deterioration of the structural quality of the films.

Magnetization measurements performed with a superconducting quantum interference device exhibit the familiar GdN ferromagnetic response for highly doped films [23]. The Curie temperature (T_C) of all films is near 65–70 K with the expected saturation magnetization M_{sat} of $\sim 7.0 \pm 0.5\ \mu_B$ for a half-filled 4f shell. In order to further investigate in detail the effect of the structural properties on the magnetic properties of GdN films we will focus on 2 samples, one having a small and one a large FWHM rocking curve value. Sample A is a 16 nm thick GdN film with a rocking curve FWHM of $13'' \times 10^3$ and sample B is a 120 nm thick GdN film with a rocking curve FWHM of $3.2'' \times 10^3$. XRD measurements show that the two films are fully relaxed and no evidence of impurity phases is found. Fig. 5(a) and (b) shows the in-plane field cooled (FC) and zero field-cooled (ZFC) magnetization of sample A and sample B under an applied field of 250 Oe, respectively. We observe reversibility between the FC and ZFC magnetization for sample B, while for sample A the ZFC magnetization shows an

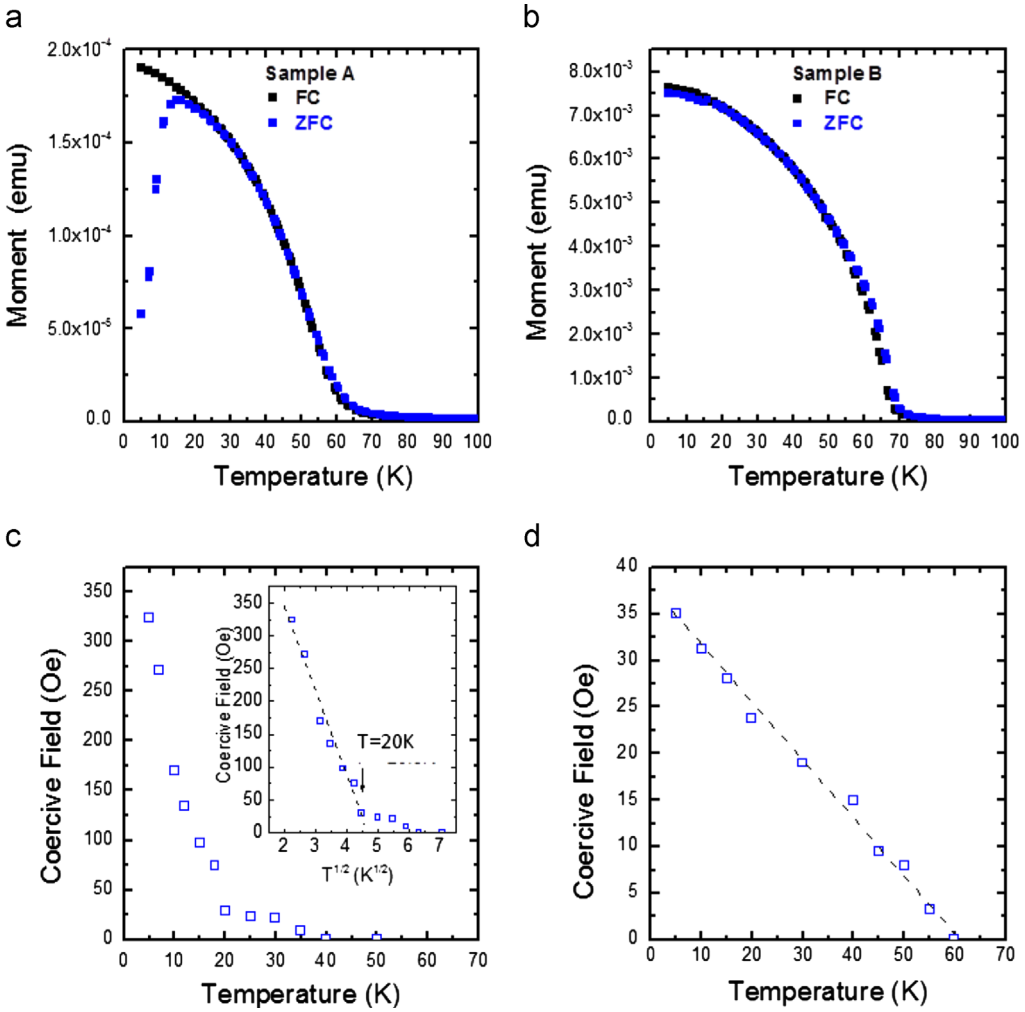

Fig. 5. In-plane field cooled (FC) and zero field-cooled (ZFC) magnetization of (a) 16 nm thick GdN and (b) 120 nm thick GdN under an applied field of 250 Oe. Temperature dependence of the coercivity for sample A (c) and sample B (d). The inset in figure (c) shows the linear dependence of coercive field on the square root of the temperature ($T^{1/2}$).

abrupt drop below ~16–17 K giving a cusp. Clearly, below this temperature, a field of 250 Oe is not sufficient to fully rotate the magnetic moment along the magnetic field direction, signaling a difference between the magnetic anisotropy of sample A and sample B. This contrast is emphasized by the temperature dependence of the coercive field (H_C) shown in (Fig. 5(c) and (d)). We observe for sample A (Fig. 5(c)) a rapid decrease of H_C with increasing temperature, resulting in the vanishing of hysteresis above ~20 K. The temperature dependence of the coercive field can be understood by considering the crystallographic structure of the sample. STM images show a surface composed of small grains, on the order of 9.5 nm, suggesting rather a "ferromagnetic ordered nanoparticles" like structure. We believe that the peak at ~16–17 K in the ZFC magnetization signals the blocking temperature of superparamagnetism arising from the nanocrystalline structure of the films. This is further supported by the inset in Fig. 5(c), showing below 20 K the linear dependence of coercive field on the square root of the temperature ($T^{1/2}$) obtained from the relation (equation 1) $H_c=H_o(1-(T/T_B))^{1/2}$, typical of nanoparticle samples [26,27]. H_o is the coercive field at 0 K, T is the measurement temperature, and T_B is the blocking temperature. The data points are found to fit reasonably well to equation 1 for $T \leq 20\ \mathrm{K}=T_B$. The value of T_B agrees well with the temperature of the maximum moment of the ZFC curve at 16–17 K. An estimate of the magnetic anisotropy K can be obtained using the general formula for nanoparticles [27]: $T_B=KV/25k_B$ where k_B is the Boltzmann constant and V the volume of GdN grains. By considering triangular grains having a base width of 9.5 nm and height of 16 nm, we calculate a magnetic anisotropy of $\sim 4\times 10^5$ erg/cm^3. A much higher value for the anisotropy of 5×10^6 erg/cm^3 has been reported for nanocrystalline GdN thin films though the authors suggested that strain might have enhanced the anisotropy [28], while a much smaller value of 2.5×10^4 erg/cm^3 has been calculated for GdN [29]. Above T_B, a rather small coercive field vanishing at 40 K is observed that could suggest the presence of a small population of grains either ferromagnetic or with a higher blocking temperature. A coercive field of only 35 Oe at 5 K is measured for sample B, about 7 times smaller than that of sample A. Once again, we can interpret this result from a crystallographic point of view. The larger the grain size, the smaller the coercive field [1,30]. More interesting is the linear temperature dependence of the coercive field for this film. This scenario seems to follow the model proposed by Gaunt for continuous films where the ferromagnetic domain walls are pinned by a random array of inhomogeneities such as dislocations or grain boundaries [30]. According to this model, which includes thermal activation, a linear dependence of H_c as a function of the temperature implies weak domain wall pinning. The vanishing of hysteresis above 50 K coincides well with the separation of the FC and ZFC curves when measured under an applied field of 20 Oe (not shown). This result is consistent with the recent work done by Natali et al. which suggests that in GdN a homogeneous ferromagnetic (FM) phase

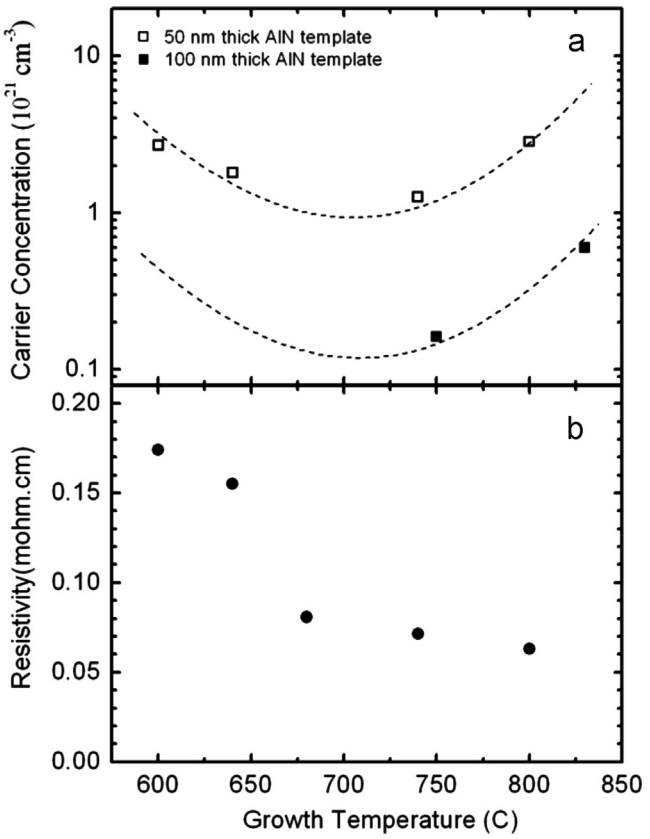

Fig. 6. (a) Ambient temperature electron carrier concentration as a function of the growth temperature for 120 nm thick GdN films grown on AlN template layers with a thickness of 50 nm (open squares) and 100 nm (solid squares). (b) Ambient resistivity as a function of the growth temperature for 120 nm thick GdN films grown on 50 nm thick AlN template layers (solid circles). The dashed lines are a guide for the eye.

exists only below 50 K, leading to the vanishing of hysteresis above this temperature [23].

We now examine the effect of the structural quality on the electrical properties of 120 nm thick GdN films grown at different temperatures on a 50 nm AlN buffer layer. Fig. 6(b) shows the variation of resistivity of the films measured at 300 K in the van der Pauw configuration as a function of the growth temperature. Such low values of resistivity, $\sim 10^{-2}$ mΩ cm, have been already reported in the literature for unintentionally doped epitaxial GdN layers and have been associated with a background electron carrier concentration ranging from 10^{20} to 10^{22} cm^{-3} originating from V_N [9,23]. The electron carrier concentration of our GdN films (measured by Hall effect in the same configuration) as a function of the growth temperature is also shown in Fig. 6(a) (open squares). The initial decline of the carrier concentration with higher growth temperatures can thus be explained by the decreased V_N concentration. The V_N concentration rises at growth temperatures above 750 °C may be associated with the escape of nitrogen from the growth surface due to the small activation energy of V_N. Remarkably, this is a similar trend with the growth temperature to that of the rocking curve FWHM reported in Fig. 4. This concomitant result, showing a strong correlation between the structural properties and the carrier concentration, suggests that V_N may be more easily trapped at grain boundaries and dislocations. This hypothesis is further supported by the higher resistivity and lower carrier concentration of 120 nm thick GdN films grown on a 100 nm thick AlN buffer layer. As discussed earlier, such thin films have a better structural quality than those grown on 50 nm thick AlN buffer layer. Electron carrier concentration reduced by a factor up to 10 is observed for the sample grown at 750 °C while a resistivity on the order of 5 mΩ cm is measured. Finally, the electrical characteristic suggests that the resistivity is the result of a more complex interplay between carrier concentration and mobility involving a strong structural dependence rather than a dependence on carrier concentration alone. Further investigations will clearly be of interest.

4. Conclusion

To summarize, we have investigated the growth by MBE of GdN thin films. It is shown that both the growth temperature of GdN and the thickness of the AlN buffer layer contribute strongly to the structural quality of the film. Our results also show a strong correlation between the structural quality and the electrical and magnetic properties of the films. In addition, the interpretation we provide may explain the origin of some of the significant differences revealed by recently published data on the conductive and magnetic states of REN thin films.

Acknowledgements

We acknowledge funding from the NZ FRST (Grant no. VICX0808), the Marsden Fund (Grant nos. 08-VUW-030 and 13-VUW-1309), and the MacDiarmid Institute for Advanced Materials and Nanotechnology, funded by the New Zealand Centres of Research Excellence Fund. We acknowledge support from GANEX (ANR-11-LABX-0014). GANEX belongs to the public funded "Investissements d'Avenir" program managed by the French Agence Nationale de la Recherche (ANR).

References

[1] F. Natali, B.J. Ruck, N.O.V. Plank, H.J. Trodahl, S. Granville, C. Meyer, W.R. L. Lambrecht, Prog. Mater. Sci. 58 (2013) 1316.
[2] B.J. Ruck, in: F. Nasirpouri, A. Nogaret (Eds.), Nanomagnetism and Spintronics, World Scientific, Singapore, 2009.
[3] K. Senapati, M.G. Blamire, Z.H. Barber, Nat. Mater. 10 (2011) 849.
[4] M.G. Blamire, A. Pal, Z.H. Barber, K. Senapati, Proc. SPIE 8461 (2013) 84610J (Spintronics V).
[5] H. Warring, B.J. Ruck, H.J. Trodahl, F. Natali, Appl. Phys. Lett. 102 (2013) 132409.
[6] S. Krishnamoorthy, T. Kent, J. Yang, P.S. Park, R.C. Myers, S. Rajan, Nano Lett. 13 (2013) 2570.
[7] A. Kandala, A. Richardella, D.W. Rench, D.M. Zhang, T.C. Flanagan, N. Samarth, arXiv:1212.1225, 2013.
[8] W.K. Liu, M.B. Santos, Thin Films: Heteroepitaxial Systems (Eds.), World Scientific Publishing Company, Singapore, 1999.
[9] M.A. Scarpulla, C.S. Gallinat, S. Mack, J.S. Speck, A.C. Gossard, J. Cryst. Growth 311 (2009) 1239.
[10] F. Natali, N.O.V. Plank, J. Galipaud, B.J. Ruck, H.J. Trodahl, F. Semond, S. Sorieul, L. Hirsch, J. Cryst. Growth 312 (2010) 3583.
[11] T.F. Kent, J. Yang, L. Yang, M.J. Mills, R.C. Myers, Appl. Phys. Lett. 100 (2012) 152111.
[12] R. Vidyasagar, S. Kitayama, H. Yoshitomi, T. Kita, T. Sakurai, H. Ohta, Appl. Phys. Lett. 100 (2012) 232410.
[13] F. Natali, B. Ludbrook, J. Galipaud, N. Plank, S. Granville, A. Preston, B.L. Do, J. Richter, I. Farrell, R. Reeves, S. Durbin, J. Trodahl, B. Ruck, Phys. Status Solidi C 9 (2012) 605.
[14] E.-M. Anton, B.J. Ruck, C. Meyer, F. Natali, H. Warring, F. Wilhelm, A. Rogalev, V.N. Antonov, H.J. Trodahl, Phys. Rev. B 87 (2013) 134414.
[15] J.H. Richter, B.J. Ruck, M. Simpson, F. Natali, N.O.V. Plank, M. Azeem, H.J. Trodahl, A.R.H. Preston, B. Chen, J. McNulty, K.E. Smith, A. Tadich, B. Cowie, A. Svane, M. van Schilfgaarde, W.R.L. Lambrecht, Phys. Rev. B 84 (2011) 235120.
[16] Do Le binh, B.J. Ruck, F. Natali, H. Warring, H.J. Trodahl, E.-M. Anton, C. Meyer, L. Ranno, F. Wilhelm, A. Rogalev, Phys. Rev. Lett. 111 (2013) 167206.
[17] F. Semond, Y. Cordier, N. Grandjean, F. Natali, B. Damilano, S. Vézian, J. Massies, Phys. Status Solidi A 188 (2001) 501.
[18] T.L. Goodrich, Z. Cai, K.S. Ziemer, Appl. Surf. Sci. 254 (2008) 3191.
[19] M.W. Cho, A. Setiawan, H.J. Ko, S.K. Hong, T. Yao, Semicond. Sci. Technol. 20 (2005) S13.
[20] E.A. Paisley, T.C. Shelton, S. Mita, R. Collazo, H.M. Christen, Z. Sitar, M.D. Biegalski, J.-P. Maria, Appl. Phys. Lett. 88 (2006) 212906.

[21] Y. Cordier, J.-C. Moreno, N. Baron, E. Frayssinet, J.-M. Chauveau, M. Nemoz, B. Damilano, F. Semond, J. Cryst. Growth 312 (2010) 2683.
[22] A. Punya, T. Cheiwchanchamnangij, A. Thiess, W.R.L. Lambrecht, Mater. Res. Soc. Symp. Proc. (2011), http://dx.doi.org/10.1557/opl.2011.383.
[23] F. Natali, B.J. Ruck, H.J. Trodahl, S. Do Le Binh, B. Vézian, Y. Damilano, F. Cordier, Semond, C. Meyer, Phys. Rev. B 87 (2013) 035202.
[24] N.O.V. Plank, F. Natali, J. Galipaud, J. Richter, M. Simpson, H.J. Trodahl, B.J. Ruck, Appl. Phys. Lett. 98 (2011) 112503.
[25] K. Senapati, T. Fix, M.E. Vickers, M.G. Blamire, Z.H. Barber, Phys. Rev. B 83 (2011) 014403.
[26] E.F. Kneller, F.E. Luborsky, J. Appl. Phys. 34 (1963) 656.
[27] M. Knobel, W.C. Nunes, L.M. Socolovsky, E. De Biasi, J.M. Vargas, J.C. Denardin., J. Nanosci. Nanotechnol. 8 (2008) 2836.
[28] K. Khazen, H.J. von Bardeleben, J.L. Cantin, A. Bittar, S. Granville, H.J. Trodahl, B.J. Ruck, Phys. Rev. B 74 (2006) 245330.
[29] S. Abdelouahed, M. Alouani, Phys. Rev. B 79 (2009) 054406;
M. Alouani, Private Communication (2013).
[30] P. Gaunt, Philos. Mag. B 48 (1983) 261;
X. Chen, P. Gaunt, J. Appl. Phys. 65 (1989) 3980.